

# Chemical Science

Accepted Manuscript



This article can be cited before page numbers have been issued, to do this please use: H. Tao, X. Sun, S. Back, Z. Han, Q. Zhu, A. Robertson, T. Ma, Q. Fan, B. Han, Y. Jung and Z. Sun, *Chem. Sci.*, 2017, DOI: 10.1039/C7SC03018E.



This is an Accepted Manuscript, which has been through the Royal Society of Chemistry peer review process and has been accepted for publication.

Accepted Manuscripts are published online shortly after acceptance, before technical editing, formatting and proof reading. Using this free service, authors can make their results available to the community, in citable form, before we publish the edited article. We will replace this Accepted Manuscript with the edited and formatted Advance Article as soon as it is available.

You can find more information about Accepted Manuscripts in the [author guidelines](#).

Please note that technical editing may introduce minor changes to the text and/or graphics, which may alter content. The journal's standard [Terms & Conditions](#) and the ethical guidelines, outlined in our [author and reviewer resource centre](#), still apply. In no event shall the Royal Society of Chemistry be held responsible for any errors or omissions in this Accepted Manuscript or any consequences arising from the use of any information it contains.



Journal Name

## ARTICLE

# Doping Palladium with Tellurium for Highly Selective Electrocatalytic Reduction of Aqueous CO<sub>2</sub> to CO

Hengcong Tao,<sup>†a</sup> Xiaofu Sun,<sup>†b</sup> Seoin Back,<sup>c</sup> Zishan Han,<sup>a</sup> Qinggong Zhu,<sup>b</sup> Alex W. Robertson,<sup>d</sup> Tao Ma,<sup>a</sup> Qun Fan,<sup>a</sup> Buxing Han,<sup>\*b</sup> Yousung Jung<sup>\*c</sup> and Zhenyu Sun<sup>\*a</sup>

Received 00th January 20xx,  
Accepted 00th January 20xx

DOI: 10.1039/x0xx00000x

www.rsc.org/

Designing highly selective and energy-efficient electrocatalysts to minimize the competitive hydrogen evolution reaction in electrochemical reduction of aqueous CO<sub>2</sub> remains a challenge. In this study, we report that doping of Pd with a small amount of Te could selectively convert CO<sub>2</sub> to CO with a low overpotential. The PdTe/few-layer graphene (FLG) catalyst with a Pd/Te molar ratio of 1:0.05 displayed a maximum CO Faradaic efficiency of about 90% at -0.8 V (vs. reversible hydrogen electrode, RHE), CO partial current density of 4.4 mA cm<sup>-2</sup> and CO formation turnover frequency of 0.14 s<sup>-1</sup> at -1.0 V (vs. RHE), which were 3.7-, 4.3-, and 10-fold higher than that over Pd/FLG, respectively. Density functional calculations showed that Te adatoms preferentially bind at terrace sites of Pd, thereby suppressing undesired hydrogen evolution, whereas CO<sub>2</sub> adsorption and activation occurred on the high index sites of Pd to produce CO.

## Introduction

Steady increases in atmospheric levels of CO<sub>2</sub> and increasing energy demands have intensified concerns about adverse CO<sub>2</sub> effects on climate change and energy supplies. Electrochemical reduction of CO<sub>2</sub> to value-added fuels and chemicals using renewable energy resources (solar, tidal, wind) provides a “clean” and efficient way to mitigating energy shortage and lowering global carbon footprint.<sup>1</sup> Nonetheless, the linear molecule CO<sub>2</sub> is stable and chemically inert with a low electron affinity and a large energy gap (13.7 eV) between its lowest unoccupied molecular orbital (LUMO) and highest occupied molecular orbital (HOMO). CO<sub>2</sub> transformation is dominated by nucleophilic attacks at the carbon, which is an uphill process requiring a substantial input of energy (~ 750 kJ mol<sup>-1</sup> required for dissociation of C=O bond). A variety of metallic electrodes have been developed to accelerate such kinetically slow reduction reaction, and the product distribution is strongly dependent on the nature of the electrode surface. Despite recent advances achieved in the electrocatalytic reduction of CO<sub>2</sub>, this field still faces challenges of 1) large overpotential (or low energetic efficiency); 2) slow electron transfer kinetics,

resulting in low exchange current densities; 3) unsatisfactory selectivity, implying a costly separation step.<sup>2-4</sup> In addition, proton reduction to evolve H<sub>2</sub> usually occurs as a severe competitive reaction especially in aqueous electrolytes, affecting CO<sub>2</sub> reduction selectivity and efficiency.

The electrochemical reduction of CO<sub>2</sub> to CO is a simple two-electron transfer process. By transferring a concerted proton-electron (H<sup>+</sup>/e<sup>-</sup>) from solution to adsorbed species, a CO<sub>2</sub> molecule is reduced to a carboxyl intermediate \*COOH. Another possible route to generate \*COOH is through a decoupled electron and proton transfer, involving the formation of a CO<sub>2</sub><sup>•-</sup> radical that is adsorbed at electrode surface. A second H<sup>+</sup>/e<sup>-</sup> can subsequently attack the oxygen atom (OH) in the \*COOH to form H<sub>2</sub>O (l) and CO.<sup>5</sup> Metals such as Au, Ag, Zn and Pd bind \*COOH tightly enough for further reduction to yield \*CO intermediate. The \*CO is weakly bound to the electrode surface, and CO desorbs from the electrode as a major product.<sup>6,7</sup> Recently, Bao et al. demonstrated a size effect of Pd particles on the electrocatalytic reduction of CO<sub>2</sub>. The Faradaic efficiency for CO production over 10.3 nm nanoparticles (NPs) was reported to be only 5.8% at -0.89 V (vs. reversible hydrogen electrode, RHE).<sup>2</sup> In addition to control of size, tuning the surface strain of Pd<sup>8</sup> and alloying with a second metal (Pd-Au,<sup>9</sup> Pd-Ni,<sup>10</sup> Pd-Cu,<sup>11,12</sup> and Pd-Pt<sup>13,14</sup>) can enhance energy efficiency and CO selectivity for CO<sub>2</sub> reduction. Density functional theory (DFT) calculations have revealed that low coordinate sites (corners/edges) of Pd particles facilitate CO<sub>2</sub> adsorption and formation of \*COOH, compared with terrace sites.<sup>2</sup> From this scenario, addition of foreign metal adatoms to tailor the electronic and geometric properties of Pd nanocrystals can substantially modify their corresponding catalytic activities. However, there have been limited studies on CO<sub>2</sub> reduction over metal NPs regarding the impact of doping

<sup>a</sup>State Key Laboratory of Organic-Inorganic Composites, Beijing University of Chemical Technology, Beijing 100029, China. E-mail: sunzy@mail.buct.edu.cn

<sup>b</sup>Beijing National Laboratory for Molecular Sciences, Key Laboratory of Colloid and Interface and Thermodynamics, Institute of Chemistry, Chinese Academy of Sciences, Beijing 100190, China. E-mail: hanbx@iccas.ac.cn

<sup>c</sup>Graduate School of EEWS, Korea Advanced Institute of Science and Technology (KAIST), Daejeon 34141, Republic of Korea. E-mail: ysjn@kaist.ac.kr

<sup>d</sup>Department of Materials, University of Oxford, Oxford, OX1 3PH, United Kingdom

<sup>†</sup>These authors contributed equally to this work.

Electronic Supplementary Information (ESI) available: Experimental details, TEM and HRTEM images, XPS survey, linear sweep voltammetry, cyclic voltammograms, Faradaic efficiency, and DFT calculation details. See DOI: 10.1039/x0xx00000x



## ARTICLE

## Journal Name

effects, and further understanding about the doping effects at the atomic level is very interesting.

We report herein that doping Pd nanocrystals with Te significantly enhances electrochemical reduction of aqueous CO<sub>2</sub> to CO, affording a much higher CO Faradaic efficiency (FE), CO partial current density, mass activity, and formation turnover frequency with respect to undoped Pd catalyst. DFT calculations reveal that Te adatoms preferentially bind at terrace sites of Pd, which can suppress unwanted hydrogen evolution in aqueous electrolysis.

## Results and discussion

Pd NPs doped with Te were supported onto the surface of few-layer graphene (FLG) by using ultrasonication-facilitated reduction of PdCl<sub>2</sub> and TeCl<sub>4</sub> precursor mixture. No capping ligands are used during the process, resulting in clean surfaces for the NPs and avoiding the problem that the stabilizer molecules adversely affect particle properties. The X-ray diffraction (XRD) patterns of Pd/FLG and PdTe/FLG are given in Fig. 1a, and Figs. S1 and S2 (Supporting Information). All of them showed four pronounced diffraction peaks at approximately 40.1°, 46.7°, 68.1°, and 81.8°, corresponding well to the (111), (200), (220) and (311) planes of face-centered cubic (fcc) Pd (PDF#46-1043), respectively. The (111) reflection is shifted toward lower 2θ after Te doping (inset of Fig. 1a, and Fig. S1b, Supporting Information), which may be caused by the lattice mismatch upon surface decoration or by the presence of interstitial heteroatoms (H or Te).<sup>15,16</sup> The average crystallite sizes were estimated to be about 8.3 and 11.0 nm for 30 wt% Pd/FLG and 30 wt% PdTe<sub>0.05</sub>/FLG respectively, from the (111) reflection utilizing Scherrer's Equation relating the coherently scattering domains with Bragg peak widths:  $L = k\lambda/B\cos(\theta)$ , in which  $k = 0.89$  for spherical particles and  $B$  is the full angular width at half-maximum of the peak in radians.<sup>17</sup> We noted that the particle size increased upon introduction of Te in Pd, which amounts to about 14.7 nm at the Te/Pd atomic ratio of 0.15 (Fig. S3, Supporting Information). Additionally, improving the loading content of PdTe led to an increase in particle sizes (Fig. S3, Supporting Information).

**Fig. 1** (a) XRD patterns, (b) Pd 3d and (c) Te 3d XPS spectra, and (d) CO FTIR spectra of 30 wt% Pd/FLG (top) and 30 wt% PdTe<sub>0.05</sub>/FLG (bottom). The bottom panel in (a) shows reference patterns for Te (hollow column, #18-1324) and metallic Pd (solid column, #46-1043).

X-ray photoelectron spectroscopy (XPS) was employed to provide insight into the surface composition of the resulting PdTe/FLG (Fig. 1b and 1c, and Fig. S4, Supporting Information). The Pd 3d XPS spectrum of PdTe/FLG (top panel in Fig. 1b) consists of asymmetric Pd 3d<sub>5/2</sub> and 3d<sub>3/2</sub> peaks centered at 335.3 and 340.6 eV, respectively, characteristic of Pd<sup>0</sup>.<sup>18</sup> The Pd 3d binding energies (BEs) of PdTe/FLG are shifted to higher values compared with the BEs of Pd/FLG (bottom panel in Fig. 1b), suggesting electron transfer from Pd to Te.<sup>19</sup> This implies that the Pd *d*-band center shifts down when Pd is doped with Te according to the *d*-band theory.<sup>20-22</sup> The Te 3d XPS spectrum (Fig. 1c) exhibited peaks at 573.8 eV (Te 3d<sub>5/2</sub>) and 583.5 eV (Te 3d<sub>3/2</sub>), indicative of Te<sup>0</sup>. The other weaker doublets at higher BEs displayed in Fig. 1b and 1c are associated with Pd<sup>2+</sup> and Te<sup>4+</sup>, respectively, which may result from the slight oxidation of the corresponding metal in contact with air.<sup>17,23</sup>

Probing CO adsorbed on Pd nanoparticle surfaces by Fourier transform infrared (FTIR) spectroscopy allows one to examine the Pd surface features modified by the Te adatoms. In Pd/FLG, CO was observed to be bonded on (111) terrace Pd<sup>0</sup> sites at ~1970 cm<sup>-1</sup> in a bridging mode (top panel in Fig. 1d).<sup>24,25</sup> However, there is no discernible bridging CO peak at a 1:0.05 mole ratio of Pd to Te (bottom panel in Fig. 1b), indicating full coverage of possibly most terrace sites at such a low Te doping level to block the active sites for the hydrogen evolution reaction.<sup>15</sup>

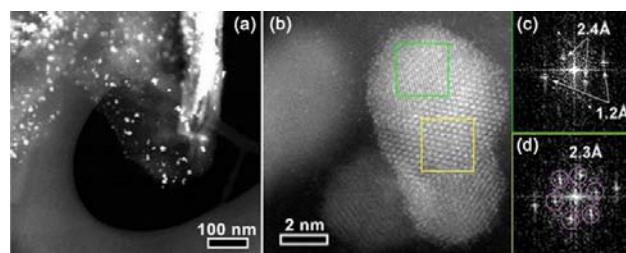
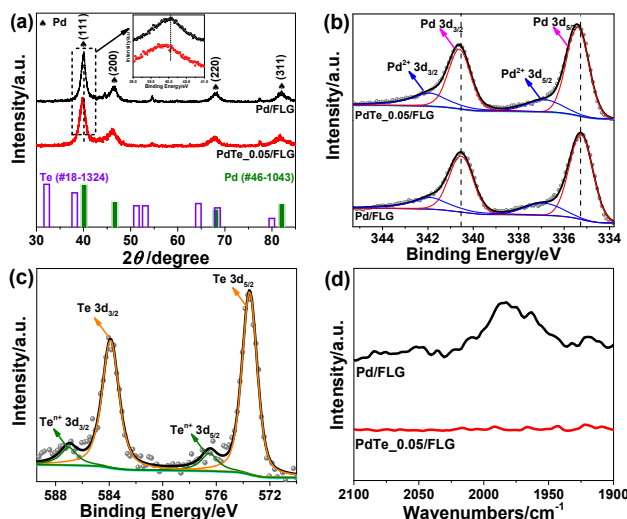


**Fig. 2** (a) Low-, and (b) high-magnification STEM images of 30 wt% PdTe<sub>0.05</sub>/FLG. The bright white streak on the right side of the FLG shown in image a is likely due to the possibility that part of the FLG is folded up. (c) and (d) Fast Fourier transforms (FFTs) of the regions marked by the green and yellow squares in (b), respectively.

Typical scanning electron microscopy (SEM) images showed a large number of graphitic flakes with lateral sizes of 300 nm – 5 μm lying flat on top of each other (Figs. S5a, S6a and b, Supporting Information). No free-standing particles detached from FLG or large particle agglomerates were observed. The formation of highly dispersed PdTe NPs was confirmed by in situ energy-dispersive X-ray spectroscopy (EDX) (Fig. S2b, Supporting Information) together with elemental mapping (Fig.



S6c-e, Supporting Information). High-angle annular dark field scanning TEM (HAADF-STEM) observation showed that isolated crystalline NPs were evenly distributed on the surface of the FLG (Fig. 2a, Fig. S7d, Supporting Information). The average particle size of PdTe NPs is about 9.7 nm, slightly bigger than that of Pd NPs (~8.6 nm), agreeing reasonably with the XRD results (Fig. S9, Supporting Information). Clearly, there are two distinctive types of lattices observed in an individual crystal of Te doped Pd (Fig. 2b). EDX confirms both Pd and Te signals (Fig. S7a-c, Supporting Information). The centered crystal with a smaller lattice is covered by outer surface lattice with a larger spacing (Fig. 2c and d). The inner lattice agrees well with the (311) spacing of fcc Pd while the outer lattice with a d-spacing of about 0.24 nm corresponds to hexagonal close-packing (hcp) Te.<sup>15</sup>

CO<sub>2</sub> reduction activities of all catalysts were tested in a typical three-electrode electrochemical system. Fig. S10a and Fig. S10b show the linear sweep voltammetry (LSV) results of 30 wt% Pd/FLG and 30 wt% PdTe<sub>0.05</sub>/FLG in 0.1 M aqueous KHCO<sub>3</sub> solution saturated with argon or CO<sub>2</sub>, respectively. It can be seen that the Te-doped sample (30 wt% PdTe<sub>0.05</sub>/FLG) exhibited a more positive onset potential and a current density nearly twice as high as that of 30 wt% Pd/FLG at -1.2 V (vs. RHE) (Fig. 3a), indicating that addition of Te atoms enhanced CO<sub>2</sub> reduction reaction. Controlled potential electrolysis of CO<sub>2</sub> was further performed at potentials between -0.6 and -1.4 V (vs. RHE) in a CO<sub>2</sub>-saturated 0.1M KHCO<sub>3</sub> solution (pH 6.8) at room temperature under atmospheric pressure. Under these reaction conditions, only CO and H<sub>2</sub> were detected by gas chromatography (GC).

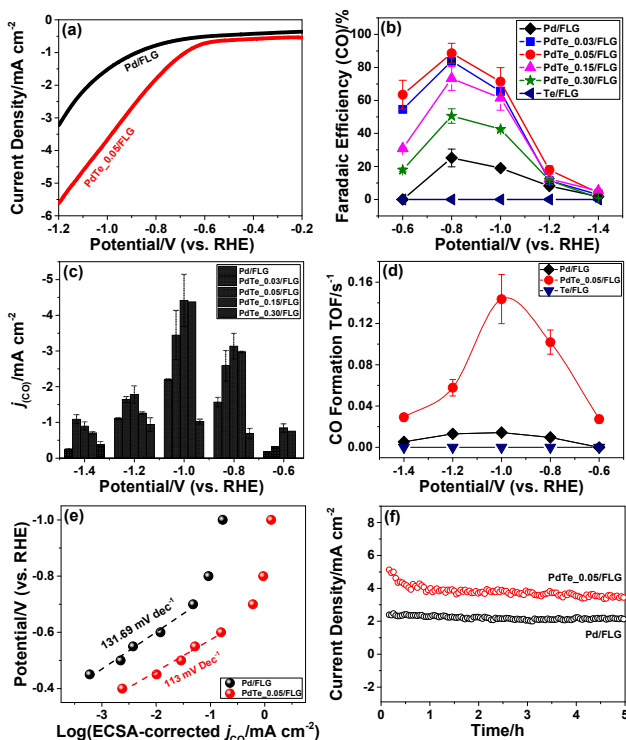


**Fig. 3** (a) LSV results of 30 wt% Pd/FLG and 30 wt% PdTe<sub>0.05</sub>/FLG electrodes in CO<sub>2</sub>-saturated 0.1 M KHCO<sub>3</sub> with a scan rate of 5 mV s<sup>-1</sup>. (b) Faradaic efficiency of CO and (c) partial current density of CO formation on Te doping ratios at various applied potentials. (d) CO formation TOF of 30 wt% Pd/FLG, 30 wt% PdTe<sub>0.05</sub>/FLG and 30 wt% Te/FLG at different applied potentials. (e) ECSA-corrected Tafel plots for CO production at applied potentials and (f) long-term durability test at -0.8 V (vs. RHE) over 30 wt% Pd/FLG and 30 wt% PdTe<sub>0.05</sub>/FLG electrodes.

The effects of Te doping content on the FE for the formation of CO at -0.6 to -1.4 V (vs. RHE) are shown in Fig. 3b. At -0.6 V (vs. RHE), 30 wt% Pd/FLG generated only H<sub>2</sub> (Fig. S11a, Supporting Information), whereas Te-doped Pd catalysts produced a mixture of CO and H<sub>2</sub> with CO selectivity of up to ~64% for the 30 wt% PdTe<sub>0.05</sub>/FLG. The CO FE increased with decreasing Te doping content at different applied potentials, reaching a maximum at Pd/Te molar ratio of 1:0.05. Further reduction in Te doping content led to a slight decrease of CO FE. Compared with Pd wire electrode exhibiting a CO FE less than 6%,<sup>26</sup> the catalysts with Pd/Te molar ratios of 1:0.03 and 1:0.05 both showed a maximum CO FE exceeding 80% at -0.8 V (vs. RHE, overpotential of 690 mV). In particular, the CO FE for the 30 wt% PdTe<sub>0.05</sub>/FLG approached ~90%, 3.7-fold higher than 30 wt% Pd/FLG. This catalyst also significantly outperforms Pd NPs of similar size (~10.3 nm) which exhibit a CO FE of only 5.8% at -0.89 V (vs. RHE, overpotential of 780 mV) as reported in literature.<sup>2</sup> Likewise, the Te-doped Pd catalysts displayed larger CO partial current densities at various reduction potentials (Fig. 3c). The mass activities of the catalysts at applied potentials followed a similar trend with their CO partial current densities, further confirming better performance of these Te-doped catalysts for CO<sub>2</sub> reduction (Fig. S11b, Supporting Information). We also found that the catalyst with a 30 wt% PdTe loading gave the highest CO FE at the applied potentials among Te-doped catalysts with a constant Pd/Te molar ratio of 1:0.05 (Fig. S12a, Supporting Information).

The CO formation turnover frequency (TOF) (Fig. 3d), a measure of pre-site activity of catalysts to produce CO, was 0.14 s<sup>-1</sup> for the 30 wt% PdTe<sub>0.05</sub>/FLG versus 0.014 s<sup>-1</sup> for 30 wt% Pd/FLG at -1.0 V (vs. RHE, overpotential of 890 mV). However, the CO formation TOF was zero for 30 wt% Te/FLG at all applied potentials, indicating that Te could not produce CO under aqueous electrolysis of CO<sub>2</sub>.

The electrocatalytically active surface area (ECSA)-corrected Tafel slope, an indication of kinetics for CO formation,<sup>27</sup> was 113 mV dec<sup>-1</sup> for 30 wt% PdTe<sub>0.05</sub>/FLG, closer to the value of 118 mV dec<sup>-1</sup> expected for rate-determining step at an electrode compared to a Tafel slope of 131.69 mV dec<sup>-1</sup> for 30 wt% Pd/FLG (Fig. 3e). This indicates that the formation of adsorbed HCOO\* intermediate on catalyst surface determines the reaction rate in both cases, but the Te-doped catalyst has better kinetics for CO<sub>2</sub> reduction.<sup>28</sup>

The long-term performances of 30 wt% PdTe<sub>0.05</sub>/FLG and 30 wt% Pd/FLG were evaluated at a constant potential of -0.8 V





(vs. RHE) for 5 h (Fig. 3f), and the current density retained 3.5 mA cm<sup>-2</sup> and 2 mA cm<sup>-2</sup>, respectively.

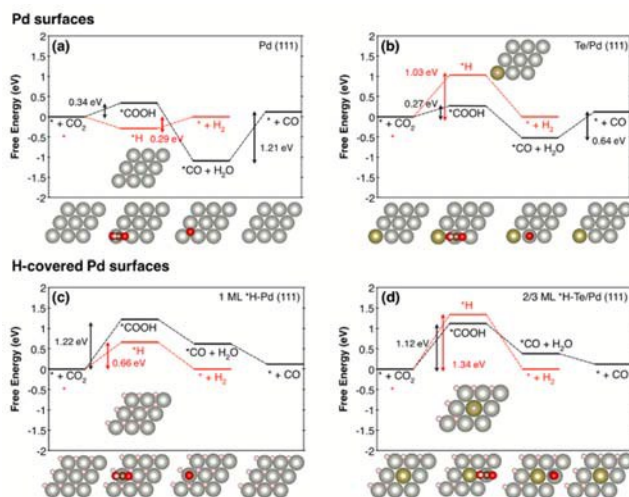


**Fig. 4** Free energy diagrams of CO<sub>2</sub> reduction to CO (black) and H<sub>2</sub> evolution reaction (red) for (a) Pd (111), (b) Te/Pd (111), (c) 1 ML \*H-Pd (111), and (d) 2/3 ML \*H-Te/Pd (111). Top views of the first layer of optimized geometries are shown. Light grey, dark grey, gold, red, white balls indicate Pd, C, Te, O, H, respectively. We note that \* represents a surface site for adsorption.

The effect of Te doping on activity and selectivity for electrochemical reduction of CO<sub>2</sub> was investigated using DFT calculations. We first compared the thermodynamic preference of Te doping on various Pd surfaces (Fig. S14), and found that the Te doping is most favourable at Pd (111) surface, which is in agreement with the XRD observation (Fig. 1a). Thus, it is reasonable to assume that Te prefers to replace Pd atom in (111) surface, and affects the catalytic properties of this surface. On the basis of this result, we modelled the Pd (111) surface with and without Te decoration. Considering that a favourable adsorption of H leads to H-covered Pd surfaces under the CO<sub>2</sub> reduction condition,<sup>29</sup> we also modelled the Pd (111) surface covered with 1 monolayer \*H and Te/Pd (111) surface covered with 2/3 monolayer of \*H, denoted as 1 ML \*H-Pd (111) and 2/3 ML \*H-Te/Pd (111), respectively (Fig. S15).

Comparing the free energy diagrams of desired CO<sub>2</sub> reduction and unwanted H<sub>2</sub> evolution reaction with and without Te decoration, we found three noteworthy points, in good agreements with the experimental measurement (Fig. 4). First, when Te is introduced to the surface layer, the energy required to form \*COOH decreased by 0.07 eV and 0.10 eV for the Pd and H-covered Pd surfaces, respectively. This result can be linked to the substantially increased experimental partial current density of CO formation of PdTe/FLG compared to Pd/FLG (Fig. 3c). Second, Te dopant facilitated the desorption of produced CO (0.64 eV), whereas this desorption step is problematic with higher desorption energy (1.21 eV) on the Pd surface. We expect that the weakening of \*CO binding on Te/Pd (111) is responsible for the absence of CO peak in FTIR spectra (Fig. 1d). Third, and most importantly, Te doping significantly destabilized

the \*H binding energies on Te top site for both Pd and H-covered Pd surfaces by 0.74 eV and 0.68 eV, respectively. We note that the geometry optimization of H adsorption with the usual three-fold hollow site (Te-Pd-Pd) as an initial geometry leads to the H atom migrating from the initial hollow site to the Pd-Pd bridge site (Fig. S15), implying the tendency of \*H to avoid Te atoms. Overall, Te doped environments tend to repel \*H adsorption and yield slightly improved CO<sub>2</sub> electrocatalysis.

With the help of the density of states analysis for Pd atom with and without Te dopant, we find that the electronic effect of Te atom on nearby Pd atom is actually not significant (Fig. S16), but the main effect of Te is rather to reduce the number of three-fold hollow sites for strong \*H adsorption. We further note that the intrinsic improvement of CO<sub>2</sub> reduction itself due to Te would not be that substantial compared to the deterioration of H<sub>2</sub> evolution, since the low coordinated stepped sites, i.e., (211) surface, are energetically more active for CO<sub>2</sub> electrocatalysis than the terrace site, and thus responsible for the catalytic activity.<sup>30</sup>

## Conclusions

In summary, we demonstrate that doping Pd with Te permits a significant enhancement in the electroreduction of aqueous CO<sub>2</sub> to CO. Te-doped Pd NPs with a Pd/Te molar ratio of 1:0.05 exhibit a CO Faradic efficiency of ~90% at -0.8 V (vs. RHE), which is 3.7-fold higher than the maximum FE of undoped Pd NPs of similar size (~24%). Such doping also allows 4.3-, and 10-fold improvement in CO partial current density and CO formation turnover frequency. DFT calculations shows that Te doping reduces the energy required to form \*COOH, weakens \*CO binding, and destabilizes \*H binding energies for both Pd and H-covered Pd surfaces. Importantly, Te adatoms preferentially bind at terrace sites of Pd, which can suppress unwanted hydrogen evolution in aqueous electrolysis, whereas CO<sub>2</sub> adsorption and activation occur on the high index sites of Pd to produce CO.

## Conflicts of interest

The authors of this manuscript have no conflicts of interest.

## Acknowledgements

This work was supported by the State Key Laboratory of Organic-Inorganic Composites (No. oic-201503005); the Fundamental Research Funds for the Central Universities (No. buctrc201525); Beijing National Laboratory for Molecular Sciences (BNLMS20160133); Key Laboratory of Photochemical Conversion and Optoelectronic Materials, TIPC, CAS; and Key Laboratory of Materials for High-Power Laser, Shanghai Institute of Optics and Fine Mechanics, CAS. Y.J. acknowledges the support through the National Research Foundation of Korea from the Korean Government (NRF-2017R1A2B3010176).

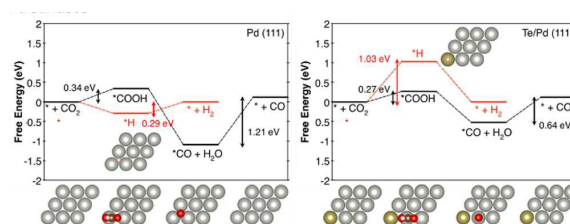


## Notes and references

1. M. Asadi, K. Kim, C. Liu, A. V. Addepalli, P. Abbasi, P. Yasaei, P. Phillips, A. Behranginia, J. M. Cerrato, R. Haasch, P. Zapol, B. Kumar, R. F. Klie, J. Abiade, L. A. Curtiss and A. Salehi-Khojin, *Science*, 2016, **353**, 467-470.
2. D. F. Gao, H. Zhou, J. Wang, S. Miao, F. Yang, G. X. Wang, J. G. Wang and X. H. Bao, *J. Am. Chem. Soc.*, 2015, **137**, 4288-4291.
3. R. Reske, H. Mistry, F. Behafarid, B. R. Cuenya and P. Strasser, *J. Am. Chem. Soc.*, 2014, **136**, 6978-6986.
4. Z. Y. Sun, T. Ma, H. C. Tao, Q. Fan and B. X. Han, *Chem*, 2017, **3**, 560-587.
5. X. W. Nie, M. R. Esopi, M. J. Janik and A. Asthagiri, *Angew. Chem. Int. Ed.*, 2013, **52**, 2459-2462.
6. S. J. Kim, W. Song, S. Kim, M. A. Kang, S. Myung, S. S. Lee, J. Lim and K. S. An, *Nanotechnology*, 2016, **27**.
7. S. B. Liu, H. B. Tao, L. Zeng, Q. Liu, Z. G. Xu, Q. X. Liu and J. L. Luo, *J. Am. Chem. Soc.*, 2017, **139**, 2160-2163.
8. H. W. Huang, H. H. Jia, Z. Liu, P. F. Gao, J. T. Zhao, Z. L. Luo, J. L. Yang and J. Zeng, *Angew. Chem. Int. Ed.*, 2017, **56**, 3594-3598.
9. R. Kortlever, I. Peters, C. Balemans, R. Kas, Y. Kwon, G. Mul and M. T. M. Koper, *Chem. Commun.*, 2016, **52**, 10229-10232.
10. S. W. Kim, M. Park, H. Kim, K. J. Yoon, J. W. Son, J. H. Lee, B. K. Kim, J. H. Lee and J. Hong, *Appl. Catal., B*, 2017, **200**, 265-273.
11. H. J. Yin and Z. Y. Tang, *Chem. Soc. Rev.*, 2016, **45**, 4873-4891.
12. H. P. Yang, S. Qin, Y. N. Yue, L. Liu, H. Wang and J. X. Lu, *Catal. Sci. Technol.*, 2016, **6**, 6490-6494.
13. R. Kortlever, I. Peters, S. Koper and M. T. M. Koper, *ACS Catal.*, 2015, **5**, 3916-3923.
14. R. Kortlever, C. Balemans, Y. Kwon and M. T. M. Koper, *Catal. Today*, 2015, **244**, 58-62.
15. S. Jones, S. M. Fairclough, M. Gordon-Brown, W. Zheng, A. Kolpin, B. Pang, W. C. H. Kuo, J. M. Smith and S. C. E. Tsang, *Chem. Commun.*, 2015, **51**, 46-49.
16. J. H. Yang, J. Yang and J. Y. Ying, *ACS Nano*, 2012, **6**, 9373-9382.
17. J. D. Cai, Y. Y. Huang and Y. L. Guo, *Appl. Catal., B*, 2014, **150**, 230-237.
18. L. X. Jiao, F. Li, X. Z. Li, R. Ren, J. Li, X. C. Zhou, J. Jin and R. Li, *Nanoscale*, 2015, **7**, 18441-18445.
19. M. H. Huang, L. R. Li and Y. L. Guo, *Electrochim. Acta*, 2009, **54**, 3303-3308.
20. K. Wu, X. B. Mao, Y. Liang, Y. Chen, Y. W. Tang, Y. M. Zhou, J. Lin, C. N. Ma and T. H. Lu, *J. Power Sources*, 2012, **219**, 258-262.
21. J. Greeley and J. K. Nørskov, *Surf. Sci.*, 2005, **592**, 104-111.
22. U. B. Demirci, *J. Power Sources*, 2007, **173**, 11-18.
23. I. Witonska, M. Frajtak and S. Karski, *Appl. Catal., A*, 2011, **401**, 73-82.
24. B. Wang, D. A. Weng, X. D. Wu and R. Ran, *Appl. Surf. Sci.*, 2011, **257**, 3878-3883.
25. S. N. Reifsnnyder, M. M. Otten and H. H. Lamb, *Catal. Today*, 1998, **39**, 317-328.
26. L. D. Burke and J. K. Casey, *J. Appl. Electrochem.*, 1993, **23**, 573-582.
27. S. Gao, Y. Lin, X. C. Jiao, Y. F. Sun, Q. Q. Luo, W. H. Zhang, D. Q. Li, J. L. Yang and Y. Xie, *Nature*, 2016, **529**, 68-71.
28. X. Q. Min and M. W. Kanan, *J. Am. Chem. Soc.*, 2015, **137**, 4701-4708.
29. D. F. Gao, H. Zhou, F. Cai, D. N. Wang, Y. F. Hu, B. Jiang, W. B. Cai, X. Q. Chen, R. Si, F. Yang, S. Miao, J. G. Wang, G. X. Wang and X. H. Bao, *Nano Res.*, 2017, **10**, 2181-2191.
30. C. Shi, H. A. Hansen, A. C. Lausche and J. K. Nørskov, *Phys. Chem. Chem. Phys.*, 2014, **16**, 4720-4727.



## TOC



Doping of Pd with a small amount of Te could selectively convert CO<sub>2</sub> to CO with a low overpotential.

